Available online at www.sciencedirect.com
SCIENCE DIRECT
Thin Solid Films 497 (2006) 135 – 141
thin solid films
www.elsevier.com/locate/tsf

Optical and non-optical characterization of Nb_2O_5–SiO_2 compositional graded-index layers and rugate structures

Robert Leitel *, Olaf Stenzel, Steffen Wilbrandt, Dieter Gäbler, Vesna Janicki, Norbert Kaiser

Optical Coatings Department, Fraunhofer Institut für Angewandte Optik und Feinmechanik, Albert-Einstein-Str. 7, 07745 Jena, Germany

Received 14 September 2004; received in revised form 20 October 2005; accepted 24 October 2005
Available online 1 December 2005

Abstract

The deposition of graded-index layers and rugate structures was performed by coevaporation of silicon dioxide as the low index material and niobium pentoxide as the high index material. To obtain information about the composition depth profile of the films, we used cross-sectional transmission electron microscopy to supplement deposition rate data recorded by two independent crystal quartz monitors during film preparation. The concentration depth profile was transformed to a refractive index profile using the effective medium approximation. The thus obtained refractive index profiles turned out to represent efficient initial approximations for re-engineering purposes.

PACS: 42.79.W; 81.15.E; 78.20.C
Keywords: Physical vapor deposition; Rugate; Gradient index; Niobium pentoxide; Silicon dioxide

1. Introduction

Optical coating designs based on layers, which are inhomogeneous along the stack axis, are known to have optical and mechanical properties that differ from those of traditional multilayer stacks. Particularly, the low optical scatter level and the wide accessible angular range make them superior to traditional stacks with respect to selected applications such as notch filters or omni-directional devices [1–4]. Manufacturing such systems requires the calculation, deposition, monitoring and characterization of optical coatings with a well-defined continuous refractive index profile perpendicular to the layer surface. Chemical vapor deposition processes have frequently been used to prepare such samples [5–7]. Conventional as well as ion assisted electron beam evaporation technology may also be used for such tasks when using coevaporation processes from two sources. Thus, the desired refractive index profile can be prepared by precisely varying the evaporation rates of both materials.

In fact, such a coevaporation process results in the deposition of mixture layers, with a refractive index, which is determined by the refractive indices of the constituents of the mixture and their concentrations. For that reason, modeling of the refractive index profile starts from the investigation of the compositional profile of the coating. Such a strategy has been applied previously in application to other coating materials [8–11], and it will be our purpose here to apply it to reverse engineering of graded-index layers and rugate structures built from Nb_2O_5 and SiO_2. We emphasize that the choice of the high refractive material Nb_2O_5 (traditionally a sputtering material [12,13]) has been stimulated by recent success to deposit high quality Nb_2O_5 layers using ion assisted electron beam evaporation with the Advanced Plasma Source APS [14].

The present study pursues reverse engineering tasks in graded-index layers and rugate structures. More concretely, the task is to determine the refractive index profile $n(\lambda,z)$ of an experimentally prepared inhomogeneous film. This cannot be done in an unambiguous manner from transmission and reflection spectra of the deposited film alone, because of the multiplicity of solutions of reverse engineering tasks from spectrophotometric data of homogeneous layer systems [15] and even more of heterogeneous coatings [16]. Instead, it is extremely helpful to utilize a priori information about the refractive index profile obtained from non-optical characterization techniques. In this paper, we demonstrate the benefits of

* Corresponding author.
E-mail address: robert.leitel@iof.fhg.de (R. Leitel).

0040-6090/$ - see front matter © 2005 Elsevier B.V. All rights reserved.
doi:10.1016/j.tsf.2005.10.064

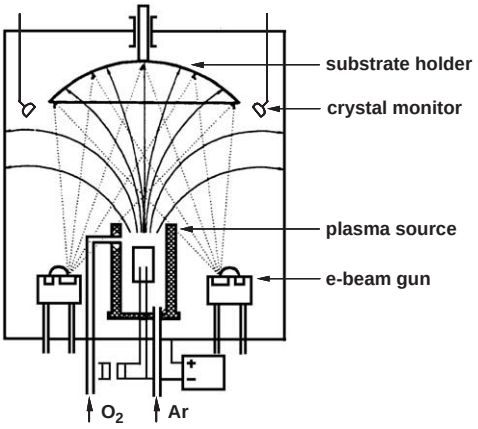

Fig. 1. Ion assisted coevaporation system.

refractive index profile determination based on deposition rate recordings during the film preparation and cross-sectional TEM investigations of the deposited film.

2. Theoretical details

Let us suppose that we deal with a material mixture built up from two materials, numbered by j. Each of the pure materials has a refractive index $n_j(\lambda)$ (where λ is the wavelength in vacuum) and occupies a thickness dependant volume fraction $V_j(z)$ of the full volume V of the mixture. Thus a volume filling factor $p_j(z)$ can be defined as a function of film thickness z:

$$p_j(z) \equiv \frac{V_j(z)}{V}; \quad \sum_{j=1}^{2} p_j(z) = 1. \tag{1}$$

The refractive index $n_m(\lambda,z)$ of the mixture may be calculated in terms of a Bruggeman's mixing formula [17] according to:

$$0 = \sum_{j=1}^{2} p_j(z) \frac{n_j^2(\lambda) - n_m^2(\lambda,z)}{n_m^2(\lambda,z) + \left(n_j^2(\lambda) - n_m^2(\lambda,z)\right)L}. \tag{2}$$

This approximation is appropriate for mixtures, where the constituents cannot be classified into inclusions and a host [18]. The depolarization factor L depends on microstructure of the composition, which is not exactly known. However, it may easily be checked that for the particular optical constants of the used mixing partners, the output of Eq. (2) does not change dramatically when L varies in an interval between 0 and 1/2, which seems reasonable for the morphology of our coatings. For convenience, in our further calculations the depolarization factor L is therefore set to a value of 1/3.

In terms of Eq. (2), the dispersion of the refractive index of the mixture follows automatically from that of the pure materials. Furthermore, if $p_j(z)$ continuously varies, the mixing formula automatically defines the spatial refractive index profile $n_m(\lambda,z)$ of the graded-index layer. Hence, knowledge on the compositional profile (represented by $p_j(z)$) allows the calculation of the refractive index profile. The refractive indices of the individual film constituents SiO_2 and Nb_2O_5 have been calculated from transmission and reflection spectra of homogeneous pure silicon dioxide and niobium pentoxide films. In the considered wavelength range, absorption losses are negligible, so only purely real indices of refraction were used for these calculations.

3. Experimental setup

Graded-index films composed of silicon dioxide and niobium pentoxide have been prepared in a Leybold Syrus-pro deposition plant by APS assisted electron beam evaporation. The films have been deposited on fused silica substrates for optical analysis and on silicon wafers for the cross-sectional TEM investigations. Fig. 1 shows a diagram of the deposition chamber. Main deposition parameters are summarized in Table 1. The deposition rates (and particularly their dependence on time) are recorded by the deposition system using two independent quartz crystal monitors. Each quartz crystal monitor is calibrated by means of tooling factors being determined from independent deposition experiments of pure silica and niobia films.

Transmission and reflection spectra of the samples on fused silica have been recorded after deposition using a Perkin Elmer Lambda900 spectrophotometer. The samples on silicon have been used for TEM cross-sectional investigations to estimate the composition of the samples from the TEM contrast.

4. Results

4.1. Negative graded-index layer

Fig. 2 (top) shows the result of the deposition rate recording during preparation of a negative graded-index layer. In this case, the refractive index of the film decreases with increasing distance from the substrate. The deposition therefore starts with a high deposition rate of niobium pentoxide and a low silicon dioxide rate. During the deposition process, the Nb_2O_5 rate was gradually decreased, while that of SiO_2 was increased. The sum of both deposition rates is also slightly increasing with time.

The relation between the niobium pentoxide and silicon dioxide deposition rates allows calculating the compositional

Table 1
Deposition parameters for graded-index layer and rugate structure

	Graded-layer	Rugate structure
Background pressure	$9.3\cdot10^{-4}$ Pa	$6.3\cdot10^{-4}$ Pa
APS working pressure	$5\cdot10^{-2}$ Pa	$4.5\cdot10^{-2}$ Pa
Oxygen flow	Constant: 35 sccm	Variable: controlled by oxygen partial pressure
APS bias voltage	140 V	140 V
Substrate temperature	150 °C	150 °C
SiO_2—rate	0…1.2 nm/s	0.9…0.5 nm/s
Nb_2O_5—rate	1.2…0.2 nm/s	0.2…0.9 nm/s
Duration of deposition	744 s	1066 s

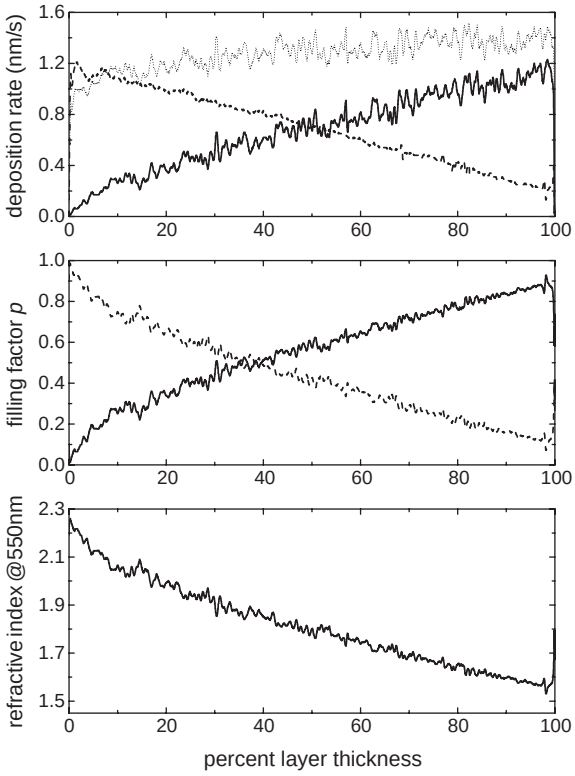

Fig. 2. Negative graded-index layer: top—deposition rates of SiO_2 (solid), Nb_2O_5 (dashed) and sum of both (dotted); center—filling factors of SiO_2 (solid) and Nb_2O_5 (dashed); bottom—refractive index profile at $\lambda = 550$ nm.

profile of the gradient layer in terms of the volume filling factors of niobium pentoxide and silicon dioxide:

$$p(Nb_2O_5) = \frac{r(Nb_2O_5)}{r(Nb_2O_5) + r(SiO_2)}$$
$$p(SiO_2) = \frac{r(SiO_2)}{r(SiO_2) + r(Nb_2O_5)} \quad (3)$$

where r is the deposition rate. The calculated compositional profiles are shown in the center of Fig. 2.

It is now straightforward to calculate the corresponding refractive index profile for any wavelength of interest by means of Eq. (2), using the filling factors obtained from Eq. (3). For the particular case of $\lambda = 550$ nm, we obtain the profile shown on bottom of Fig. 2, which shows the expected decrease of the refractive index with distance from the substrate surface.

Although the presented methodology gives direct access to the refractive index profile, one must keep in mind that the deposition rates result from an indirect monitoring procedure [19]. They are not recorded at the position of the growing film (which is held at a rotating substrate holder), but at fixed positions in the deposition chamber (see Fig. 1) and then corrected using tooling factors. Therefore, a cross-check of our results was performed, using compositional profiles obtained from TEM investigations of the samples.

A cross-sectional transmission electron micrograph of the negative graded-index sample on silicon can be seen in Fig. 3. This image reveals a dark to bright contrast that corresponds to the compositional profile of the film. Note that the effect of the substrate holder rotation and the location of the e-beam gun appear as a fine substructure in the TEM image. However, the modulation period caused by the substrate holder rotation is in the region of 3.3 nm and thus too small to affect the optical film spectra at normal incidence. It has therefore not been taken into consideration for further calculations.

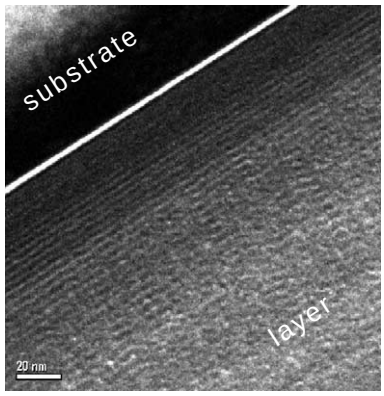

Fig. 3. Cross-sectional TEM image (high resolution nearby substrate), courtesy of Ute Kaiser, University of Ulm, Germany.

On top of Fig. 4 the TEM intensity profile is shown as resulting from the image from Fig. 3. Its shape is related to the compositional profile of the deposited materials. In order to relate this intensity profile to the material concentrations in a quantitative manner, the curve has been calibrated with respect

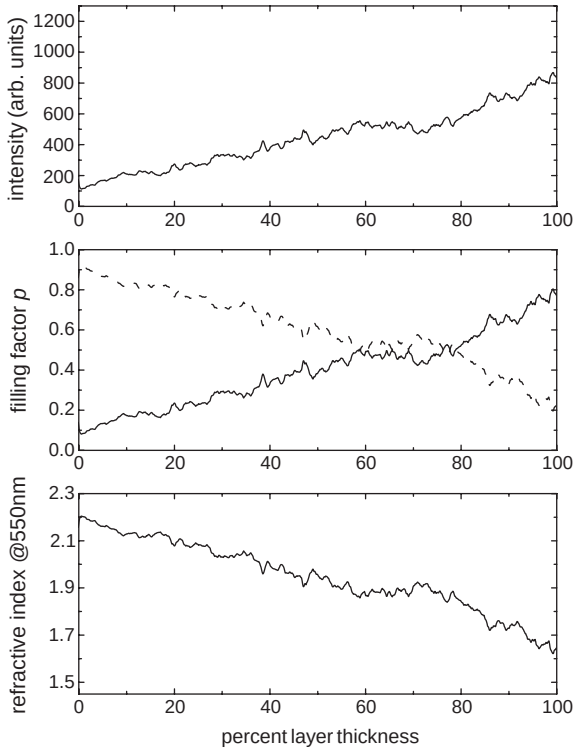

Fig. 4. Negative graded-index layer: top—intensity profile of the sample; center—filling factors of SiO_2 (solid) and Nb_2O_5 (dashed); bottom—refractive index profile at 550 nm.

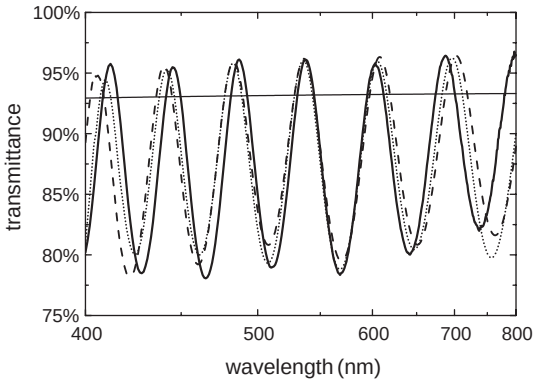

Fig. 5. Transmittance spectra of the negative graded-index layer on fused silica (measured spectrum (solid), calculated from deposition rate (dashed), calculated from TEM linescan (dotted), uncoated substrate (thin)).

to the deposition rates at the beginning and the end of the deposition. We then obtain the material concentrations as shown in Fig. 4 (center).

The corresponding refractive index profile according to Eq. (2) is plotted on the bottom of Fig. 4. It is again consistent with the produced negative index gradient, but differs in its shape from that determined from the rate recordings.

Having calculated the refractive index profiles corresponding to rate recordings and TEM images, the film spectra (transmittance or reflectance) may be calculated by any thin film calculation software. The result of the transmittance calculation is shown in Fig. 5, together with the measured spectra of the graded-index layer. The assumed thickness values are 1178 nm for the calculation based on rate-recording data, and 1097 nm for the TEM data. Both physical thickness values correspond to the same optical thickness, because the convex refractive index profile from Fig. 2 (bottom) corresponds to a lower mean refractive index than the slightly concave profile from Fig. 4 (bottom).

As shown, both calculations are in qualitative agreement to the experimental spectrum. Particularly, the transmission at the halfwave points (degree of inhomogeneity) is well reproduced, while there appear problems in reproducing the quarterwave points (lower envelope) and the correct dispersion behavior (spacings between adjacent interference extrema). The refractive index profiles determined so far may therefore be regarded as an initial approximation to the real refractive index profile.

4.2. Rugate structure

As a second example, let us discuss the refractive index profile of a periodic sequence of ten negative and positive index gradients, further referred to as rugate structure. Fig. 6 (left) shows the rate recordings during deposition, while Fig. 6 (right) shows the TEM cross-sectional image of the sample. In an identical manner as discussed for the case of the graded-index layer, we obtain the following refractive index profiles for the rugate structure (Fig. 7).

Again, both profiles resemble the intended periodic refractive index profile, although there occur differences in the obtained profile shapes. The next step is therefore to calculate the corresponding transmittance spectra, and to compare them to the measured spectrum (Fig. 8). Here, the full coating thickness has been tuned to reproduce the correct stopband position, which leads to a coating thickness of 1484 nm for the rate-recording-based calculation, and 1402 nm for the TEM-based calculation. As in the case of the graded-index layer, both profiles allow reproducing the main spectral features. However, the fine details of the measured spectrum are not reproduced yet, so that the obtained refractive index profiles again represent an initial approximation of the real behavior.

Practically, the established refractive index profiles are extremely helpful in reverse engineering tasks, because they may be used as initial approximation for re-engineering by local search methods. This is exemplified for the case of the rugate system (see Figs. 9 and 10). Indeed, from Fig. 7 one may postulate that the rugate structure may be approximated by a sequence of positive and negative linear refractive index ramps (at 550 nm wavelength, as shown in Fig. 9). In terms of this assumption, the experimental spectrum from Fig. 8 may be fitted, varying only the corner points of the mentioned triangular shaped refractive index profile. As a result, transmittance and reflectance spectra as shown in Fig. 10 are

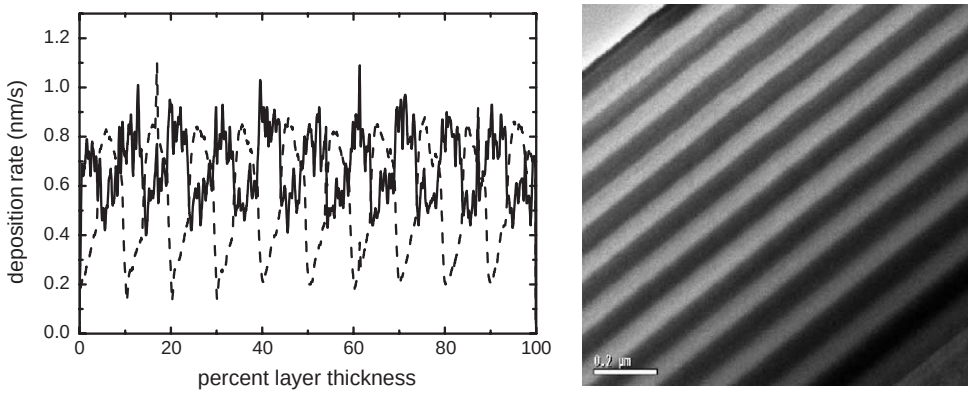

Fig. 6. Left—deposition rate vs. layer thickness (SiO_2 (solid), Nb_2O_5 (dashed)); right—cross-sectional electron micrograph of a rugate structure, courtesy of Ute Kaiser, University of Ulm, Germany.

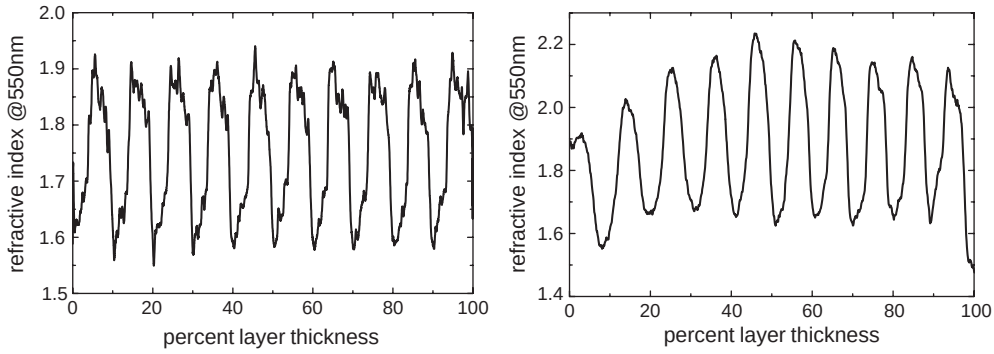

Fig. 7. Refractive index profiles of the rugate structure (left—obtained from rate recordings; right—obtained from TEM).

obtained, while the final parameters of the refractive index profile at 550 nm are given in Fig. 9.

5. Discussion

The results presented in the previous section demonstrated that non-optical data on the compositional profile of inhomogeneous layers could be used to obtain a first approximation of their refractive index profile for computation of its spectral properties. Corresponding results have been achieved from deposition rate recordings as well as TEM investigations.

The established refractive index profiles of the negative gradient reproduce the halfwave points and the amplitude of the oscillations in the transmittance spectrum, which in fact indicates that the mean refractive index and the degree of inhomogeneity are well suitable [20]. Finer details of the spectum are not reproduced yet. The same is valid for the more complex rugate structure. The refractive index gradient emerging from the deposition rate data approximates the spectral properties, particularly the stopband, quite well.

When discussing the merit of spectra reproduction, one must keep in mind that the calculations of the transmittance spectra from Figs. 5 and 8 are *not* spectra fits. The transmittance calculations discussed so far only correspond to the experimentally established compositional profiles. Furthermore, both methods (TEM and deposition rate recording) are indirect characterization methods. The reason is that the samples used for TEM investigation are not identical with those used for optical analysis, because they have been deposited onto different substrates. Rate recordings, on the other hand, are accomplished at fixed positions in the deposition chamber (see Fig. 1), and are corrected using simple tooling factors. Moreover, cross-correlations between the rate recordings for niobium pentoxide and silicon dioxide may occur due to insufficient screening of the crystal monitors from each other. All these problems are potential sources of systematic errors, so that in fact the quality of reproducing the experimental spectra is rather good.

Comparing the relative value of the rate recording and TEM data, which should be emphasized, the rate-recording data is available in real time during deposition, and may therefore be used for fast reverse engineering and even for rapid prototyping [21] of graded-index coatings. On the contrary, TEM cross-sectional investigations are time-consuming and expansive. For that reason, we favor the utilization of the rate recordings for rapid (in situ) reverse engineering of inhomogeneous coatings and rugates. Moreover, these data may be combined with in situ broadband optical spectroscopy recordings of the growing film [22], to obtain a consistent and complete picture of the growth process of any coating. Similar information may be drawn from TEM, but only with a serious time delay.

We come to the result that the sophisticated evaluation of rate recordings and TEM images is very helpful for reverse engineering of inhomogeneous optical coatings. The results are mutually consistent.

Regarding the quality of the spectra fits shown in Fig. 10, its obvious that all spectral features are well reproduced.

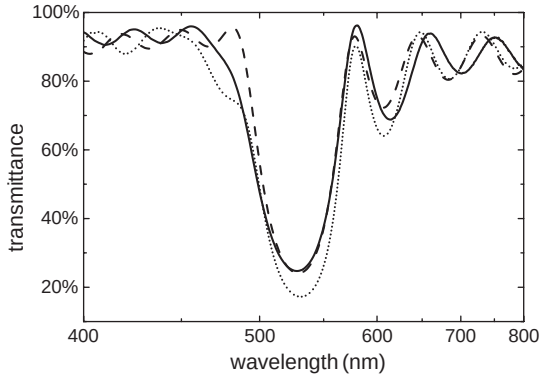

Fig. 8. Transmittance spectra of the rugate structure on fused silica (measured spectra (solid), calculated from deposition rate (dashed), calculated from TEM linescan (dotted)).

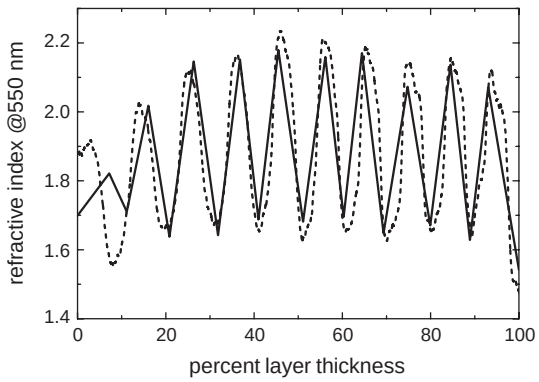

Fig. 9. Refractive index profile of the rugate from reverse engineering (solid) using TEM investigation as starting design (dashed).

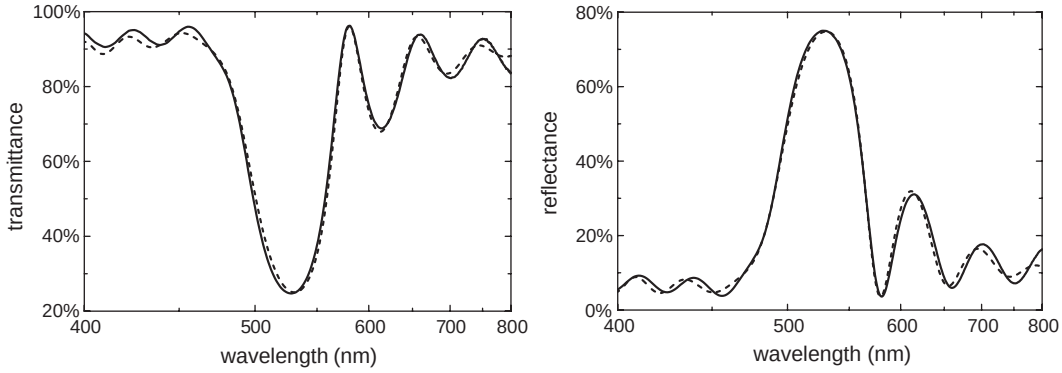

Fig. 10. Comparison of transmittance (left) and reflectance (right) spectra from measurement (solid) and reverse engineering (dashed) using TEM data as initial design.

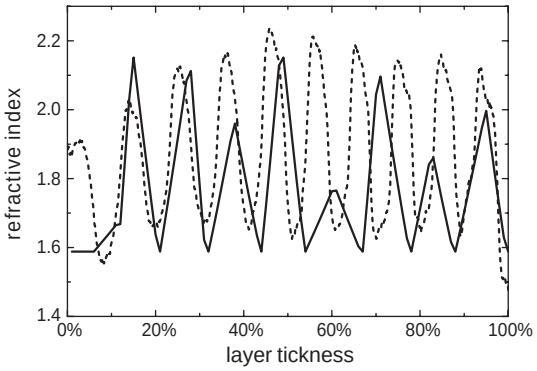

Fig. 11. Refractive index profile of the rugate from reverse engineering (solid) using the designed profile as initial approximation in comparison to the refractive index profile obtained from TEM (Fig. 9).

Unfortunately, niobia shows strong absorption losses at wavelength values below 380 nm, so it is useless to extend the fit into the UV region that makes it impossible to check the theoretical reproduction of higher harmonics of the stopband. On the other hand, it should be once more emphasized that reverse engineering from normal incidence transmission and reflection spectra leads to multiple solutions, and the decision on the physically relevant solution cannot be made on the base of the degree of spectra reproduction only. Our particular choice of initial approximation leads to a solution with a refractive index profile, which is consistent with *both* the experimental spectra and non-optical a priori information on the compositional profile. This is not generally the case, if other initial approximations are applied.

In order to illustrate the effect of multiple solutions, Fig. 11 represents another re-engineering result for the same periodic structure, obtained from the fit of transmittance and reflectance if the *designed* refractive index profile has been used as the initial approximation. Although the obtained result fits very well to the measured spectra (Fig. 12), the obtained refractive index profile is not consistent with the results of non-optical analysis, particularly with the results from TEM-investigations, as shown in Fig. 11 by the dashed line. The disagreement to the deposition rate recordings (see Fig. 7 on left) is even stronger. The most serious point is that the number of periods is wrong: The re-engineering result from Fig. 11 shows only 8 oscillations instead of 10. Clearly, such a refractive index profile is physically meaningless, although it is quite consistent with the optical spectra.

Once more, this result clarifies the well-known fact that it is impossible to identify the true re-engineering solution from the mathematical solution multiplicity basing on the merit of ex situ spectra reproduction only. Instead, any additional a priori information on the construction parameters of the system should explicitly be used in the course of the re-engineering procedure.

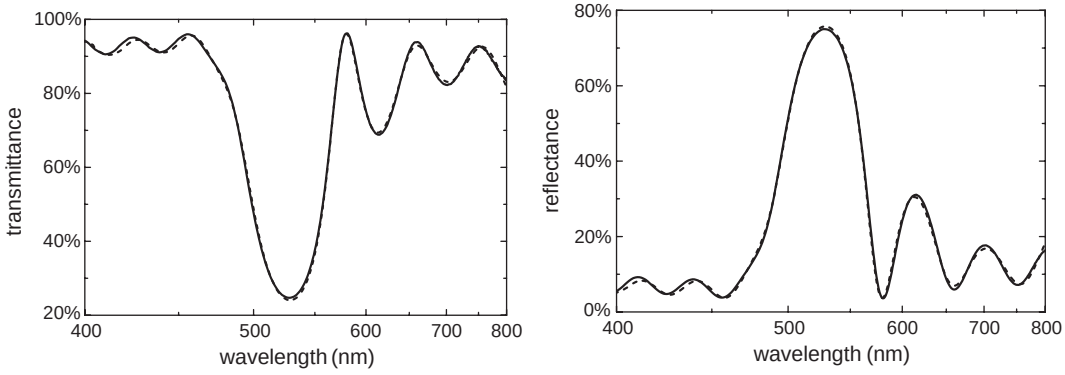

Fig. 12. Comparison of transmittance (left) and reflectance (right) spectra from measurement (solid) and reverse engineering (dashed) using the designed refractive index profile as initial approximation.

One last point concerns the choice of the mixing equation. In our study, the effective medium approximation (EMA) given by Eq. (2) was used to generate the initial approximation of the refractive index profile. Minor modifications in the profile will occur, if the depolarization factor L is altered or when the EMA is replaced by Maxwell Garnett, Lorentz–Lorenz, or Looyenga [23] mixing models. Nevertheless, all the mentioned models are only convenient approximations, because they intermix the polarizabilities of the constituents of the mixture, regarding them to be the same as in the pure materials. Therefore, they do not consider size effects, effects caused by surface chemistry, and so on. Particularly, for mixtures of the type Nb_2O_5/SiO_2, the application of an empirically found ad hoc relationship between deposition rates and optical constants may lead to an even better reproduction of the optical spectra than it is achieved using the Bruggeman formula [24]. Practically, as we use the mixing model only for generation of a starting refractive index profile for re-engineering, the concrete choice of the mixing formula seems to be less crucial a problem than the accurate determination of the compositional profile itself.

6. Summary

The refractive index profile of graded-index layers and rugate structures built from SiO_2 and Nb_2O_5 was estimated using a combination of optical and non-optical characterization techniques. For the rugate structure, TEM cross-sectional investigations delivered good quality profiles, which are consistent with the main features of the measured sample transmittance and could be used as starting approximation for the spectra fit. The same kind of information can be drawn from deposition rate recordings. On the other hand, TEM investigations cannot be used for online re-engineering during deposition, or rapid prototyping. For real time re-engineering, the goal should therefore be to combine the fast rate-recording technique with a complementary non-destructive (optical) monitoring technique to enhance the accuracy of online controlling of the film growth.

Future work will be concentrated on the replacement of the Bruggeman equation by a more suitable mixing formula, and on the implementation of a reverse engineering strategy, which combines the evaluation of rate recordings and in situ optical broadband monitoring during film deposition in real time.

Acknowledgments

The authors thank Heidi Haase for sample preparation, Dr. Ute Kaiser (University of Ulm, Germany) for TEM-performance and the BMWA for financial support. Robert Leitel acknowledges valuable discussions with Prof. Kowarschik and Prof. Richter (Friedrich Schiller University, Germany). Vesna Janicki thanks the Fraunhofer Society in Germany for a Fraunhofer Fellowship at IOF in Jena.

References

[1] A.H. Guenther, International trends in Appl. Opt. Vol. 5, SPIE Press Monograph, PM119m, 2002.
[2] A.R. Offer, J. Bland-Hawthorn, Mon. Not. R. Astron. Soc. 299 (1998) 176.
[3] R.L. Hall, W.H. Southwell, Proceedings SPIE 2046 (1993) 78.
[4] A.V. Tikhonravov, Appl. Opt. 32 (1993) 5417.
[5] D. Poitras, S. Larouche, L. Martinu, Appl. Opt. 41 (2002) 5249.
[6] P.L. Swart, P.V. Bulkin, B.M. Lacquet, Opt. Eng. 39 (1997) 1214.
[7] S. Lim, S. Shih, J.F. Wagner, Thin Solid Films 277 (1996) 144.
[8] A. Brunet-Bruneau, S. Fisson, B. Gallas, G. Vuye, J. Rivory, Proceedings SPIE 3738 (1999) 188.
[9] N. von Rottkay, T.J. Richardson, M. Rubin, J. Slack, E. Masetti, G. Dautzenberg, Proceedings SPIE 3138 (1997) 9.
[10] J.-H. Park, W.J. Cho, K.S. Hong, Proceedings SPIE 4102 (2000) 79.
[11] Y. Tsou, F.C. Ho, Appl. Opt. 35 (1996) 5091.
[12] B. Hunsche, M. Vergöhl, H. Neuhäuser, F. Klose, B. Szyszka, T. Matthée, Thin Solid Films 392 (2001) 184.
[13] K. Yoshimura, T. Miki, S. Iwama, S. Tanemura, Thin Solid Films 281/282 (1996) 235.
[14] H. Ehlers, K. Becker, R. Beckmann, et al., Proceedings SPIE 5250 (2003) 646.
[15] R.T. Phillips, J. Phys. D: Appl. Phys. 16 (1983) 489.
[16] J.P. Borogogno, B. Lazarides, E. Pelletier, Appl. Opt. 21 (1982) 4020.
[17] D.A.G. Bruggeman, Ann. Phys. 24 (1935) 636.
[18] D.E. Aspnes, J.B. Theeten, Phys. Rev., B 20 (1979) 3292.
[19] B.T. Sullivan, J.A. Dobrowolski, Appl. Opt. 31 (1992) 3821.
[20] A.V. Tikhonravov, M.K. Trubetskov, B.T. Sullivan, J.A. Dobrowolski, Appl. Opt. 36 (1997) 7188.
[21] K. Starke, T. Groß, M. Lappschies, D. Ristau, Proceedings SPIE 4094 (2000) 83.
[22] S. Wilbrandt, R. Leitel, D. Gäbler, O. Stenzel, N. Kaiser, 9th Optical Interference Coatings, Tuscon, USA, June 27–August 2, 2004.
[23] H. Looyenga, Physica 31 (1965) 401.
[24] A.V. Tikhonravov, M.K. Trubetskov, M.A. Kokarev, T.V. Amotchkina, O. Stenzel, S. Wilbrandt, D. Gäbler, N. Kaiser, 6th International Conference Appl. Opt., St. Petersburg, Russia, 2004.